Effect of MgAl$_2$O$_4$ Catalyst Support Synthesis Method on the Catalytic Activity of Nickel Nano Catalyst in Reverse Water Gas Shift Reaction

A. Ranjbar[1], S. F. Aghamiri[1], A. Irankhah[2]*

[1] *Chemical Engineering Department, Faculty of Engineering, University of Isfahan, Isfahan, Iran*
[2] *Hydrogen and Fuel Cell Research Laboratory, Department of Chemical Engineering, Faculty of Engineering, University of Kashan, Kashan, Iran*

ARTICLE INFO	ABSTRACT
	In this research, the effect of synthesis method of magnesium aluminate as the support of Ni catalysts at the reverse water gas shift (RWGS) reaction was evaluated. The RWGS reaction was applied in Carbon Dioxide Hydrogenation to form Methanol via a Reverse Water-Gas Shift Reaction (CAMERE) process im order to tranform CO$_2$ into methanol. The MgAl$_2$O$_4$ supports were prepared by sol-gel (M1), surfactant-assisted co-precipitation (M2), and ultrasonic-assisted co-precipitation (M3) techniques. Moreover, 1.5 wt % Ni/M1 showed the highest CO$_2$ conversion (42.1 %) and lowest CO selectivity, while 1.5 wt % Ni/M2 showed the lowest CO$_2$ conversion and the highest CO selectivity (> 92.5 %). The 1.5 wt % Ni/M3 showed similar catalytic activity as 1.5 wt % Ni/M2, but with lower CO selectivity. The high CO selectivity of 1.5 wt % Ni/M2 with a BET surface area of 121.7 m^2g^{-1} was accredited to a higher dispersion of Ni particles resulted by higher total pore volume of this catalyst. The high specific surface area along with large total pore volume is effective in increasing the nickel dispersity. The following pore size distribution and total pore volume order were obtained for the catalysts: 1.5 wt % Ni/M2 > 1.5 wt % Ni/M3 > 1.5 wt % Ni/M1. Among the prepared supports, M1 with BET of 174.5 $m^2.g^{-1}$ showed the highest specific surface area. All prepared supports and catalysts were of mesoporous structure. Well dispersed NiO species with high interaction with the support were detected by TPR analysis. The SEM images detected particles with less than 80 nm for M2 and 1.5 wt % Ni/M2 samples. The long-term stability test performed on 1.5 wt % Ni/M2 showed great catalytic activity after 15 h on stream.

1. Introduction

The emission of greenhouse gases, especially carbon dioxide, has increased over the last decades [1]. With the negative effects of CO$_2$ on climate change and global warming, CO$_2$ recycling is an excellent way to mitigate its atmospheric concentration. Since catalytic reactions can utilize and convert CO$_2$ into methanol or long-chain hydrocarbons, increasing interests in new catalytic reactions

---

[*]Corresponding author: sfaghamiri@gmail.com

have been witnessed [2, 3]. Reverse water gas shift (RWGS) reaction ($CO_2 + H_2 \rightarrow CO + H_2O$) is an endothermic reaction with higher efficiency than other CO_2 hydrogenation reactions. The produced CO from RWGS reaction with an excess amount of H_2 can be used as the feedstock for methanol synthesis or Fischer-Tropsch (F-T) process [4].

The RWGS reaction is accompanied by CO and CO_2 methanation reactions. The side reactions depending on the catalyst and the reaction condition could take place along with the primary reaction. Finding catalysts that suppress methanation reactions, especially at lower temperatures, has always been a challenge in catalysts for RWGS reaction. Noble metals like Pt, Pd, Rh, Au, Re [5-7] and non-noble metals such as Cu [8], Ni [9], and Co [10] have been used for RWGS reaction. Noble metals show high activity, but have low CO selectivity. Non-noble metals are more attractive economically. Among the non-noble catalysts, Ni shows high CO_2 conversion in RWGS reaction. However, Ni catalysts show low CO selectivity at high nickel contents. In other words, the Ni loading is a critical point for nickel catalysts, and low nickel content with high dispersity facilitates the RWGS reaction, while high nickel loadings intensify methanation processes [11]. The structural and chemical properties of the support also play a significant role in the activity and CO selectivity of these catalysts. The high surface area supports such as alumina and SBA-15 help the dispersity of Ni particles and consequently enhance the CO selectivity [11-14]. The oxygen storage ability of the support is widely emphasized by researchers [4, 10, 12]; therefore, nickel catalysts have also been supported on CeO_2 [12] and Mo_2C [15, 16]. An increase in CO_2 adsorption facilitates CO

selectivity in Ni catalysts, as stated by Chen et al. [13]. $MgAl_2O_4$ or magnesium aluminate spinel with its unique chemical, thermal, electrical, optical, and mechanical properties has attracted a great deal of attention [17, 18]. $MgAl_2O_4$ has been synthesized by methods like co-precipitation, sol-gel, citrate-nitrate combustion, microemulsion, and freeze drying [19-22]. The synthesis method directly affects the physical and structural properties of prepared magnesium aluminate [20]. $MgAl_2O_4$ with its essential properties and high specific surface area as a basic support can increase CO_2 adsorption and CO selectivity in Ni catalysts [23,24].

Until now, Ni catalysts supported on $MgAl_2O_4$ spinel and the effect of the $MgAl_2O_4$ support synthesis method on CO selectivity in the RWGS reaction have not been evaluated. In this research, magnesium aluminate spinels with high specific surface areas were synthesized by three different techniques (sol-gel, surfactant-assisted co-precipitation, and ultrasonic-assisted co-precipitation) and used as support for Ni catalysts to evaluate the effect of support preparation method. For an effective evaluation of support synthesis method, low nickel loadings were used. Then, 1.5 wt % Ni catalysts were prepared by the wet impregnation technique.

2. Experimental
2.1. Synthesis of $MgAl_2O_4$ by sol-gel method (M1)

For the preparation of $MgAl_2O_4$ by sol-gel method (M1), at first, citric acid ($C_6H_8O_7 > 99.5$ %, Loba Chemie) was dissolved in distilled water; then, the CTAB (Cetyl trimethylammonium bromide $C_{19}H_{42}BrN > 99$ %, Sigma-Aldrich) surfactant was added to the solution under continuous stirring to form

a transparent solution. Afterward, the precursor salts, $Mg(NO_3)_2.6H_2O$ (Magnesium nitrate hexahydrate > 98.0 %, Loba Chemie) and $Al(NO_3)_3.9H_2O$ (Aluminum nitrate nonahydrate > 98.0 %, Loba Chemie), were added to solution under continuous stirring. After the dissolution of the nitrates for better control of the final particle size, 2 ml ammonium hydroxide (NH_4OH 25 %, Loba Chemie) was added drop wise to the solution at 30 ^{o}C to adjust pH at 9. Subsequently, the mixture was stirred for another 4 h at 60 ^{o}C. The gel was dried at 80 ^{o}C for 24 h and calcined at 700 ^{o}C at a rate of 3 ^{o}C/min for 4h.

2.2. Synthesis of MgAl₂O₄ by surfactant-assisted co-precipitation (M2)

For the preparation of $MgAl_2O_4$ by surfactant-assisted co-precipitation technique (M2), $Mg(NO_3)_2.6H_2O$ and $Al(NO_3)_3.9H_2O$ were added to the transparent solution containing CTAB surfactant. Ammonia as the precipitating agent was added to the solution by pH adjustment at 10. After filtration, the precipitate was washed and dried at 80 ^{o}C for 24 h. For calcination, the same procedure as the sol-gel method was used.

2.3. Synthesis of MgAl₂O₄ by ultrasonic-assisted co-precipitation (M3)

The ultrasonic-assisted precipitation technique (M3) was the same as the surfactant-assisted co-precipitation technique except that, during the precipitation step, the ultrasonic was used. Similar drying and calcination conditions to M2 were used for the M3 sample.

2.4. Catalyst preparation

Nickel catalysts were prepared by the wet impregnation technique, as reported by Ranjbar et al. [25].

2.5. Catalyst characterization method

The XRD patterns were recorded on an X-ray diffractometer (PANalytical X'Pert-Pro) in the range of $2\theta = 10°$ to $80°$. The obtained patterns were compared with the Joint Committee on Powder Diffraction Standards (JCPDS). Powder diffraction file No. 01-1157 for $MgAl_2O_4$ and No. 89-7101 for NiO were used for comparison. The BET surface areas and pore structure of samples were measured using a Micromeritics Tristar 3000 analyzer through the adsorption of N_2 at −196 ^{o}C. Scanning Electron Microscopy (SEM) was performed with VEGA TESCAN, operating at 30 kV. The temperature-programmed reduction profile (TPR) was obtained by using Micromeritics AutoChem 2920 TPR apparatus in the temperature range of 30 to 1000 ^{o}C at a rate of 10 ^{o}C/min at a flow rate of 20 ml/min of 5 vol % H_2/Ar. The catalyst samples were degassed under inert atmosphere of Ar at 200 ^{o}C before conducting the TPR analysis.

2.6. Catalyst testing method and apparatus

A continuous flow fixed bed reactor (8-mm-i.d.) made of quartz tube was used for evaluating the catalytic activity. For each test, the reactor was loaded with 100 mg of catalyst. The catalysts were reduced in situ under H_2 flow (30 ml/min) at 600 °C for 4 h and cooled down to 400 °C in flow of Argon before the reaction. Total flow of 60 ml/min consisting of $H_2:CO_2=1:1$ was inserted as feed into the reactor. Mass flow controllers (Brooks instruments model SLA-5850S) were used for monitoring the inlet flow. The reactor was confined by a three-zone heating jacket (model SOTELEM, 220 V) with temperature indicator and controller (TIC) systems (model JUMO BITRON08). Activity

tests were carried out at temperatures ranging from 400 to 700 °C in steps of 100 °C, and each test was repeated three times at each temperature. The outlet flow of the reactor passed through a cold trap to condense and remove water from the product stream. The product stream was analyzed by a gas chromatograph (model 8A-Shimadzu) equipped with a thermal conductivity detector (TCD) and a Carbosieve column. The process flow diagram of the experimental apparatus is shown in Fig. 1.
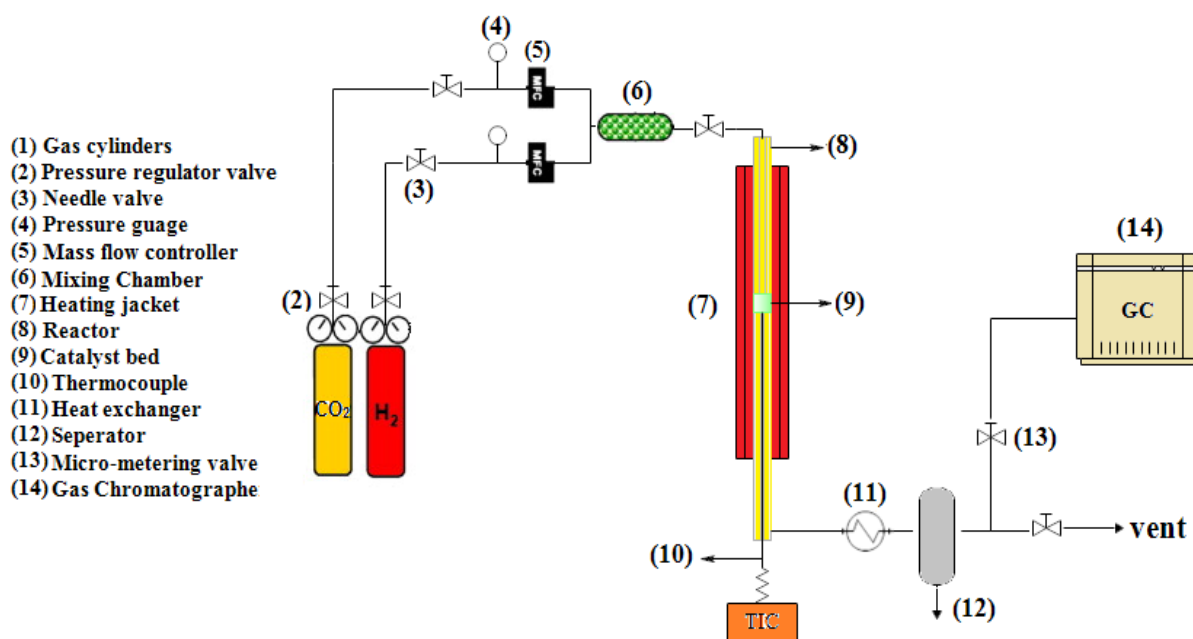
(1) Gas cylinders
(2) Pressure regulator valve
(3) Needle valve
(4) Pressure guage
(5) Mass flow controller
(6) Mixing Chamber
(7) Heating jacket
(8) Reactor
(9) Catalyst bed
(10) Thermocouple
(11) Heat exchanger
(12) Seperator
(13) Micro-metering valve
(14) Gas Chromatographe

Figure 1. Process flow diagram of experimental apparatus for the evaluation of Ni catalysts in the reverse water gas shift reaction.

3. Results and discussion

3.1. Supports and catalyst characterizations

Figure 2 shows the XRD patterns of prepared supports and catalysts. As can be seen, pure crystalline $MgAl_2O_4$ phase is formed for all the prepared samples (JCPDF No. 075-1796). Crystallite sizes of prepared samples are calculated on (311), (400), and (411) planes from the half-width of diffraction peaks (β) using Scherrer's formula, Eq. 1.

$$D= 0.9\lambda/\beta Cos\theta \qquad (1)$$

In XRD patterns of catalysts, no peak related to NiO could be detected, which is due to low Ni loading.

The structural properties of supports and catalysts are presented in Table 1. M1 showed the highest specific surface area (174.5 m2.g-1), but the lowest total pore volume (0.2149 cm3g-1) and mean pore size (4.9 nm). M2 and M3 showed almost the same specific surface areas. As can be seen in Table 1, a slightly smaller total pore volume and mean pore diameter is observed for M3 sample and its associated catalyst. The impregnation of the supports with Ni decreased the specific surface areas in all samples; however, still, the 1.5 wt % Ni supported on M1 showed the highest surface area in the prepared catalysts. Yet, there is no obvious connection between the SBET value and pore volume of catalysts, while 1.5 wt % Ni/M1 and 1.5 wt % Ni/M2 showed the lowest and highest pore volume/S_{BET} ratios, respectively.
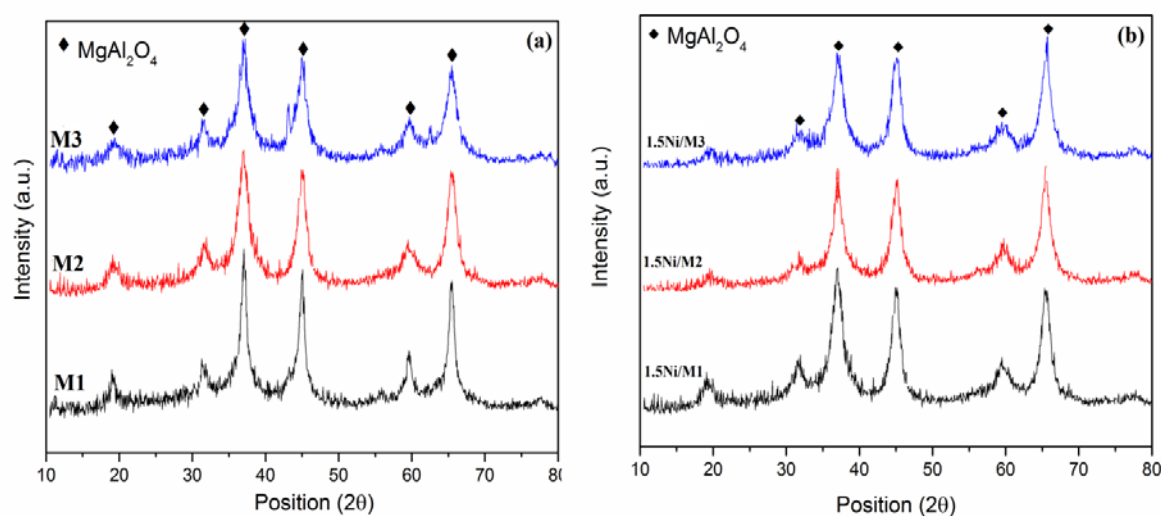
Figure 2. XRD patterns of different prepared supports and catalysts.

Table 1
Structural properties of the different prepared catalysts and support samples.

Sample	BET $(m^2.g^{-1})$	Total pore volume $(cm^3\ g^{-1})$	Mean pore size (nm)	Pore volume/S_{BET} $(\times 10^{-9}\ m)$	Crystallite size (nm)		
					311	400	440
M1	174.5	0.2149	4.9	-	14.7	9.4	9.2
M2	151.1	0.7176	18.9	-	14.8	15.1	13.8
M3	153.3	0.6915	18.1	-	10.5	12.6	11.8
1.5Ni/M1	155.1	0.1434	3.8	9.25	-		
1.5Ni/M2	121.7	0.5226	17.4	42.7	-		
1.5Ni/M3	124.2	0.4978	16.8	39.4	-		

[a] calculated from XRD patterns.

Figs. 3a and 3c reveal the pore size distribution of the prepared supports and catalysts, respectively. The prepared supports and catalysts show mesoporous pore size distribution. M1 support shows smaller total pore volume and narrower pore size distribution than those of M2 and M3. The nitrogen adsorption/desorption isotherms of supports and catalysts are shown in Figs. 3b and d, respectively. According to the IUPAC classification for M1 and 1.5 wt % Ni/M1, the N_2 isotherm is a type IV isotherm with a type H4 hysteresis loop. The H4 loop is a composite of types I and II, the more pronounced uptake at low p/p^0 is associated with the filling of micropores [26]. For M2, M3, 1.5 wt % Ni/M2 and 1.5 wt % Ni/M3, the N_2 isotherm is a type IV isotherm with a type H3 hysteresis loop. Most catalysts and their oxide carriers belong to this class of isotherm [27].

Fig. 4 shows the TPR profile of 1.5 wt % Ni/M2 catalyst. The reduction of catalyst occurs in a range of 550 to 900 °C. There is a small peak at temperatures lower than 550 °C, which is attributed to disperse NiO with high interaction with the support. The peak at 800 °C is attributed to the incorporation of NiO with the support or its higher interaction with $MgAl_2O_4$.
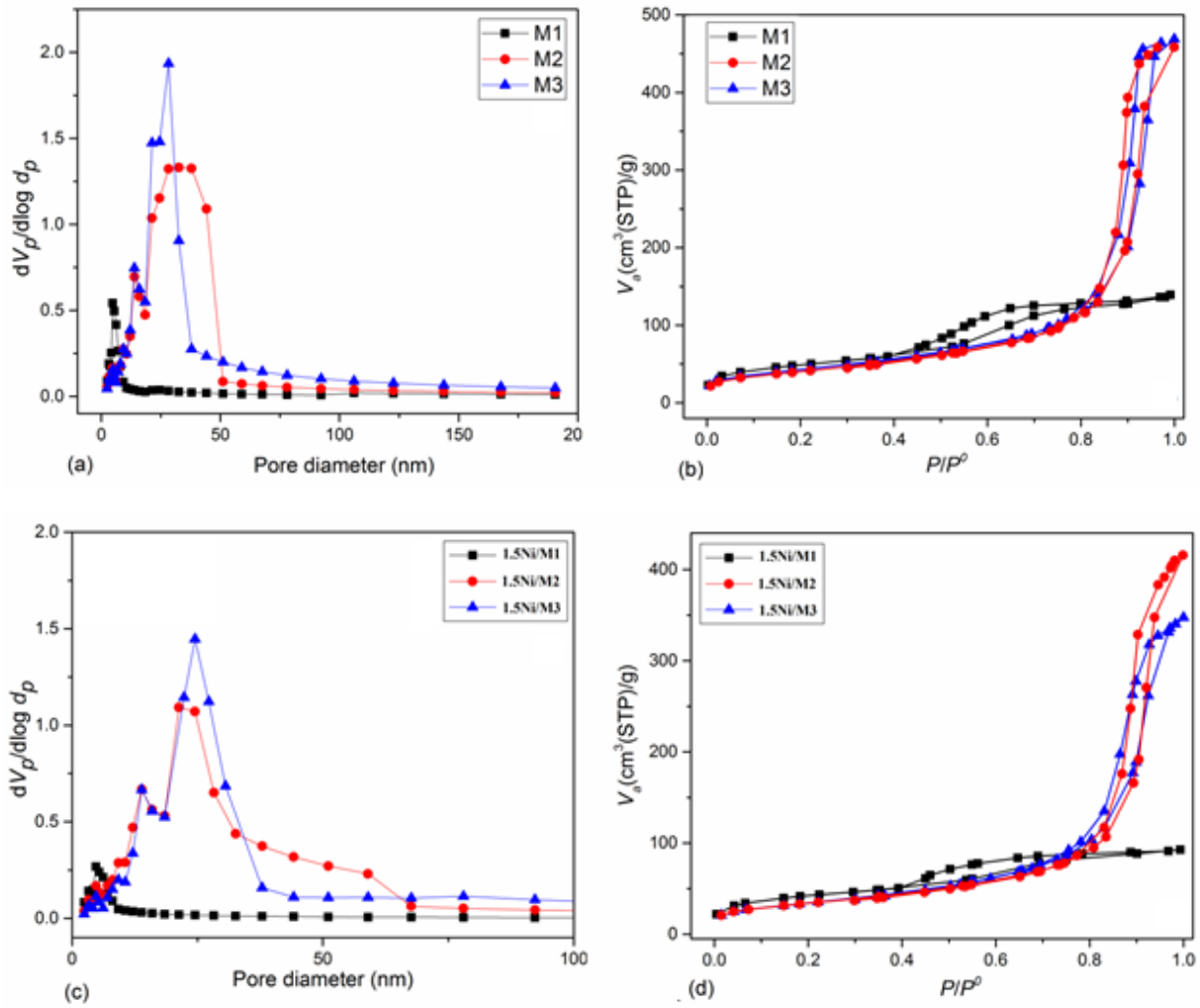
Figure 3. (a) Pore size distribution of prepared M1, M2, and M3 (b) N2 adsorption/desorption isotherms of prepared supports, (c) Pore size distribution of prepared catalysts, and (d) N2 adsorption/desorption isotherms of prepared catalysts.
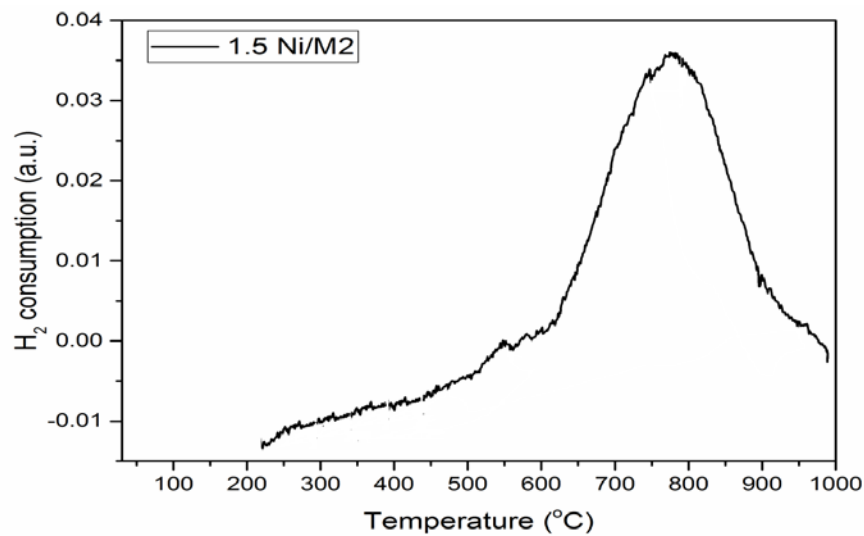

Figure 4. TPR profile of 1.5 wt % Ni/M2 catalyst with 10 % vol H_2/Ar, heating rate 10 ^{o}C/min.

Figure 5 shows SEM images of M2 support, 1.5 wt % Ni/M2 catalyst, and the EDS analysis of 1.5 wt % Ni/M2. The particles in the support and catalyst do not possess any particular shape, but have a similar size distribution. The average particle size of the support and catalyst is calculated by Digimizer Software by using more than 100 particles. The support and catalyst showed average particle size of 62 and 78 nm, respectively. The EDS analysis of 1.5 wt % Ni/M2 (fig. c) confirmed the presence of elements in the catalyst and showed 1.71 wt % nickel in the catalyst.
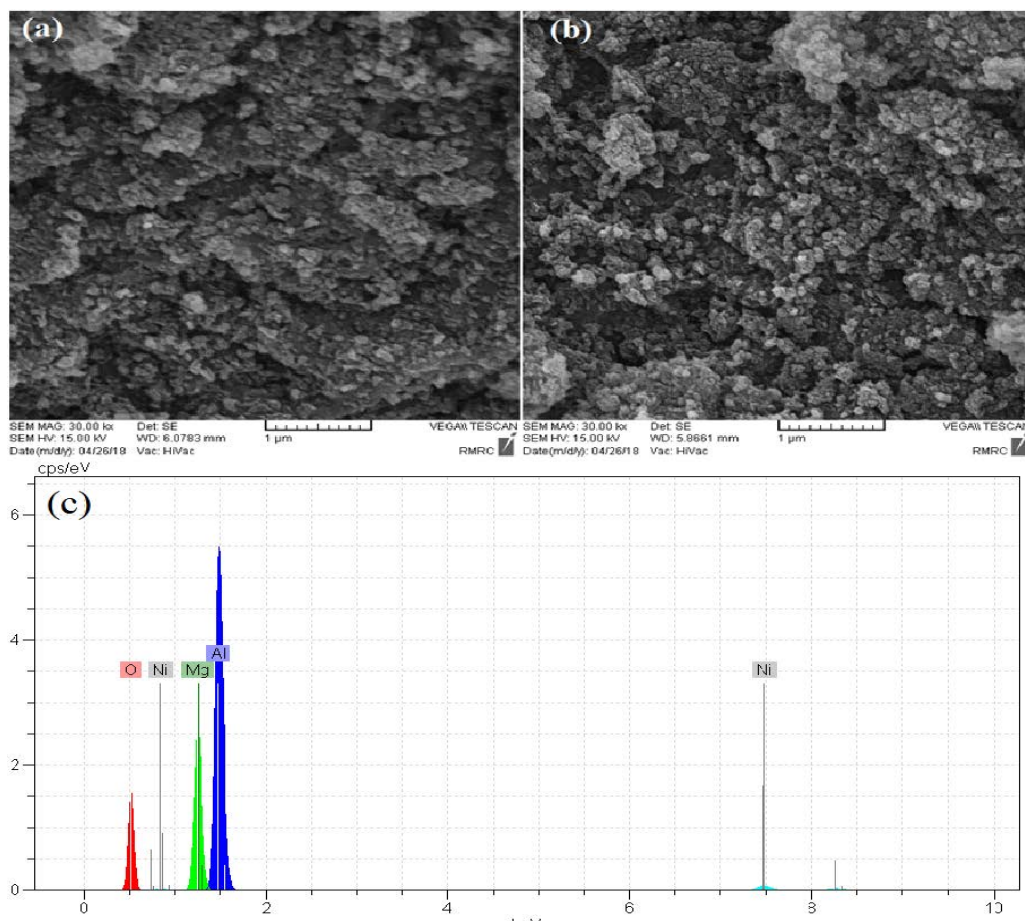

Figure 5. SEM images of (a) M2 support, (b) 1.5 wt % Ni/M2 catalyst, and (c) EDS analysis of 1.5 wt % Ni/M2.

3.2. Catalytic reaction performance

The CO_2 conversion, CO and CH_4 selectivity over 1.5 wt % Ni catalysts at different temperatures are shown in Figures 6a, 6b, and 6c, respectively. High CO_2 conversion and CO selectivity (> 80 %) were observed for all the prepared catalysts. The high activity and CO selectivity of these catalysts were contributed to the high basicity of the $MgAl_2O_4$ supports and Ni dispersion. As can be seen in Figs. 6a & 6b, the highest CO_2 conversion and the lowest CO selectivity at all temperatures were obtained for 1.5 wt % Ni/M1. CO_2 conversion of 42.1 % at 700 °C was obtained for 1.5 wt % Ni /M1. In addition, 1.5 wt % Ni on M2 and M3 showed almost the same CO_2 conversion, but, for 1.5 wt % Ni/M2, slightly higher CO selectivity was observed. High activity and CO selectivity of 1.5 wt % Ni/M2 in comparison

with 1.5 wt % Ni on M1 and M3 was attributed to the higher dispersion of Ni particles on the M2 support. The CO selectivity increased by high Ni dispersion or small nickel particle size. A direct relation between the pore volume/S_{BET} ratio and the Ni dispersion was observed. This ratio decreased in the following order 1.5 wt % Ni/M2 > 1.5 wt % Ni/M3 > 1.5 wt % Ni/M1, which was in accordance with the CO selectivity of these catalysts. Although the highest specific surface area was possessed by 1.5 wt % Ni/M1, it showed the lowest total pore volume, which affected the Ni dispersity. An increase in the Ni dispersion is caused by high specific area along with an increase in the total pore volume [28]. These observations are consistent with the results reported by other researchers [29]. Due to the high hydrogen coverage on the active sites of Ni particles with low dispersity and large size, the methanation processes occurring along with the RWGS reaction are encouraged [11, 14].

The high basicity of magnesium aluminate is confirmed by many researchers using analysis like CO_2-TPD [30, 31]. The CO_2 adsorption and CO formation increase on the basic support. Formate dissociation mechanism is the leading mechanism proposed for RWGS reaction [32]. According to this mechanism, both formate formation and dissociation are increased with the enhancement of CO_2 adsorption. Consequently, CO production is increased due to an increase in formate dissociation. In addition to CO formation, the CO desorption step has been also accepted as an essential step in CO selectivity. If CO is stuck to active sites, it is then followed by CO methanation reaction ($CO + 3H_2 \leftrightarrow CH_4 + H_2O$). In other words, a consecutive pathway is assumed for the CO methanation. The CO methanation reaction is also intensified with large and agglomerated particles.

Findings for 1.5 wt % Ni/MgAl$_2$O$_4$ catalysts were compared with those of the Ni catalysts reported in the literature, and results are given in Table 2. As can be seen, the prepared catalysts in the present work showed high CO_2 conversion and excellent CO selectivity (> 99.9 % at 700 ^{o}C for 1.5 wt % Ni/M2) in comparison with the reported Ni catalysts.

The long term stability test of 1.5 wt % Ni/M2 at 600 ^{o}C is shown in Figure 7 after 15 h of testing 1.5 wt % Ni on M2 support in reaction stream; the catalyst showed stable CO_2 conversion and high CO selectivity (> 98 %).
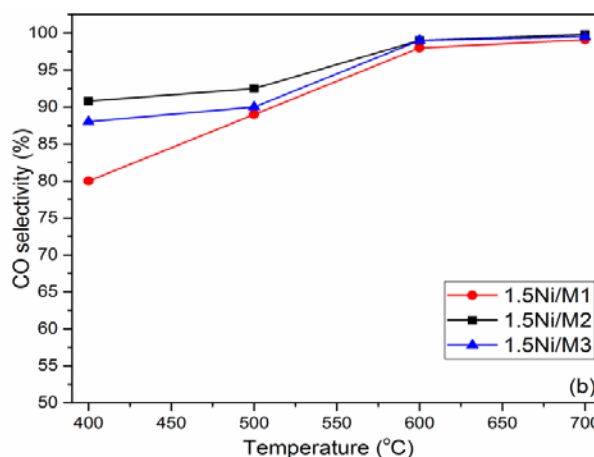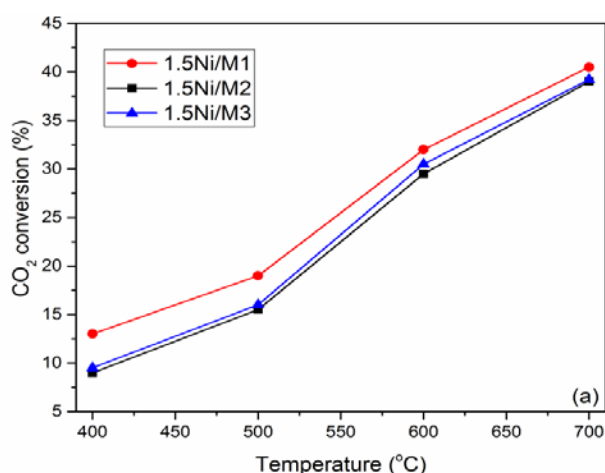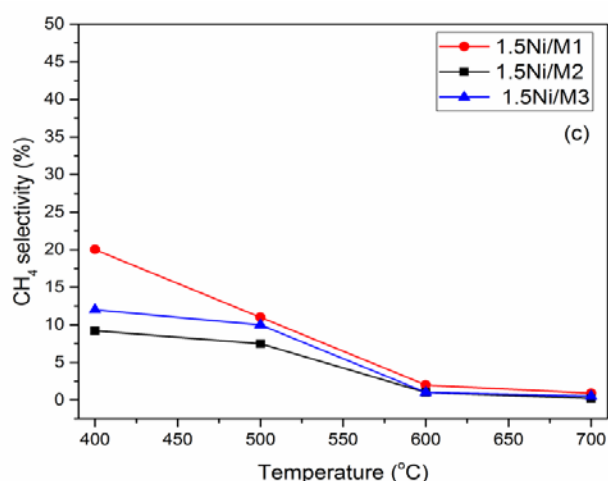
Figure 6. (a) CO_2 conversion, (b) CO selectivity, and (c) CH_4 selectivity of 1.5 wt % Ni on M1, M2, and M3 at different temperatures; H_2:CO_2 =1:1 (GHSV= 2.4× 10⁴ ml.g⁻¹.h⁻¹).

Table 2
Comparison of results obtained from the present study and the literature for Ni catalysts.

| Catalyst	Synthesis method	T (°C)	P (bar)	H₂:CO₂	CO₂ conv. (%)	CO sel. (%)	Ref.
	Sol gel				42.1	> 98	
Ni/MgAl₂O₄	Co- pre.	700	1	1:1	39.2	> 99.9	Present work
	Ultra co-pre.				39.5	> 99	
Ni/CeO₂	Co-precipitation	700	1	1:1	40	> 90	Liu et al. [9]
Ni/SBA-15	Hydrothermal	900	1	1:1	55	100	Lu et al. [11]
Ni-K/Al₂O₃	impregnation	500	1	1:1	-	> 70	Chen et al. [13]
Ni/ B-Mo₂C	CVD	200	1	5:1	8	37	Zhang et al. [16]
Ni/Ce-Al	Impregnation	750	1	4:1	> 60	> 90	Yang et al. [4]
Cu-Ni/Al₂O₃	Polymeric method	700	-	1:1	20	-	Loretie et al. [33]
Ni/Ce-Zr	Co-precipitation	750	1	1:1	45	> 95	Sun et al. [34]
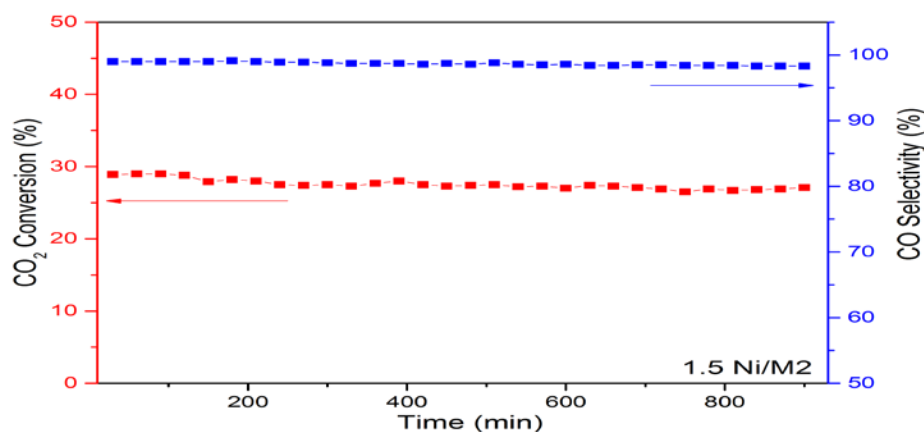
Figure 7. Long-term stability test of 1.5 wt % Ni/M2, reaction temperature: 600 °C, H_2:CO_2 =1:1 (GHSV= 1.5× 10⁴ ml.g⁻¹.h⁻¹).

4. Conclusions

Nanocrystalline $MgAl_2O_4$ as support for nickel-based catalysts was synthesized through three different synthesis techniques: 1) sol-gel (M1), 2) surfactant-assisted co-precipitation (M2), and 3) ultrasonic-assisted co-precipitation (M3) techniques. Then, 1.5 wt % Ni catalysts were investigated in RWGS reaction. All prepared catalysts showed CO selectivity higher than 80 % at all investigated temperatures. The structural and physical properties of synthesized supports and catalysts directly affected the CO selectivity in the catalysts. All prepared catalysts showed high CO_2 conversion (> 39.2 %). Moreover, 1.5 wt % Ni/M2 and high CO_2 conversion showed the best CO selectivity (> 92 %) at all studied temperatures. The high CO selectivity of 1.5 wt % Ni/M2 catalyst was contributed to high specific surface area along with large total pore volume. The pore volume/S_{BET} ratio had a direct relation with the Ni dispersion and CO selectivity in RWGS reaction. This ratio decreased in the following order: 1.5 wt % Ni/M2 > 1.5 wt % Ni/M3 > 1.5 wt % Ni/M1. All prepared samples possessed the mesoporous structure. No particular shape was observed for M2 and 1.5 wt % Ni/M2 by SEM analysis. The elemental decomposition analysis (EDS) showed 1.71 wt % Ni on M2 support. After 15 h of testing 1.5 wt % Ni on M2 support in reaction stream, it showed high and stable catalytic performance.

Nomenclature

β	the full width at half maximum intensity of the peak [Rad].
BET	Brunauer-Emmett-Teller [$m^2.g^{-1}$].
CAMERE	carbon dioxide hydrogenation to form methanol via a reverse water-gas shift reaction.
D	crystallite size [10^{-9} m].
EDS	energy dispersive X-ray spectrometry.
GC	gas chromatography.
GHSV	gas hourly space velocity [$ml.g^{-1}.h^{-1}$].
IUPAC	the international union of pure and applied chemistry.
JCPDS	joint committee on powder diffraction standards.
λ	X-ray wavelength [10^{-10} m].
M1	$MgAl_2O_4$ prepared by the sol-gel technique.
M2	$MgAl_2O_4$ prepared by a surfactant-assisted co-precipitation technique.
M3	$MgAl_2O_4$ prepared by ultrasonic-assisted co-precipitation technique.
RWGS	reverse water gas shift.
SEM	scanning electron microscopy.
TCD	thermal conductivity detector.
TIC	temperature indicator and controller.
TPR	temperature-programmed reduction.
Wt.%	weight percent.
XRD	X-ray diffraction.

References

[1] Florides, G. A. and Christodoulides, P., "Global warming and carbon dioxide through sciences", *Environ. Int.*, **35** (2), 390 (2009).

[2] Davis, B. H., "Fischer-Tropsch synthesis: Current mechanism and futuristic needs", *Fuel Process. Technol.*, **71** (1-3), 157 (2001).

[3] Gogate, M. R. and Davis, R. J., "Comparative study of CO and CO_2 hydrogenation over supported Rh-Fe catalysts", *Catal. Commun.*, **11** (10), 901 (2010).

[4] Yang, L., Pastor-Pérez, L., Gu, S., Sepúlveda-Escribano, A. and Reina, T. R., "Highly efficient $Ni/CeO_2-Al_2O_3$ catalysts for CO_2 upgrading via reverse water-gas shift: Effect of selected transition metal promoters", *Appl. Catal. B Environ.*, **232**, 464 (2018).

[5] Panaritis, C., Edake, M., Couillard, M., Einakchi, R. and Baranova, E. A., "Insight towards the role of ceria-based supports for reverse water gas shift reaction over RuFe nanoparticles", *J.*

CO₂ Util., **26**, 350 (2018).

[6] Kim, S. S., Lee, H. H. and Hong, S. C., "The effect of the morphological characteristics of TiO_2 supports on the reverse water-gas shift reaction over Pt/TiO_2 catalysts", *Appl. Catal. B Environ.,* **119**, 100 (2012).

[7] Goguet, A., Meunier, F., Breen, J., Burch, R., Petch, M. I. and Ghenciu, A. F., "Study of the origin of the deactivation of a Pt/CeO_2 catalyst during reverse water gas shift (RWGS) reaction", *J. Catal.*, **226** (2), 382 (2004).

[8] Chen, C. S., Cheng, W. H. and Lin, S. S., "Mechanism of CO formation in reverse water-gas shift reaction over Cu/Al_2O_3 catalyst", *Catal. Lett.*, **68** (1-2), 45 (2000).

[9] Wang, L., Liu, H., Liu, Y., Chen, Y. and Yang, S., "Influence of preparation method on performance of $Ni\text{-}CeO_2$ catalysts for reverse water-gas shift reaction", *J. Rare Earth.*, **31** (6), 559 (2013).

[10] Wang, L., Liu, H., Chen, Y., Zhang, R. and Yang, S., "K-Promoted $Co\text{-}CeO_2$ catalyst for the reverse water-gas shift reaction", *Chem. Lett.*, **42** (7), 682 (2013).

[11] Lu, B. and Kawamoto, K., "Preparation of monodispersed NiO particles in SBA-15, and its enhanced selectivity for reverse water gas shift reaction", *J. Environ. Chem. Eng.*, **1** (3), 300 (2013).

[12] Dai, B., Zhou, G., Ge, S., Xie, H., Jiao, Z., Zhang, G. and Zhang, X., "CO_2 reverse water-gas shift reaction on mesoporous $M\text{-}CeO_2$ catalysts", *Can. J. Chem. Eng.*, **95** (4), 634 (2017).

[13] Chen, C. S., Lin, J. H., You, J. H. and Yang, K. H., "Effects of potassium on $Ni\text{-}K/Al_2O_3$ catalysts in the synthesis of carbon nanofibers by catalytic hydrogenation of CO_2", *J. Phys. Chem. A*, **114** (11), 3773 (2009).

[14] Chen, C. S., Cheng, W. H. and Lin, S. S., "Study of iron-promoted Cu/SiO_2 catalyst on high temperature reverse water gas shift reaction", *Appl. Catal. A Gen.*, **257** (1), 97 (2004).

[15] Porosoff, M. D., Kattel, S., Li, W., Liu, P. and Chen, J. G., "Identifying trends and descriptors for selective CO_2 conversion to CO over transition metal carbides", *Chem.Commun.*, **51** (32), 6988 (2015).

[16] Zhang, X., Zhu, X., Lin, L., Yao, S., Zhang, M., Liu, X. and Ma, D., "Highly dispersed copper over $\beta\text{-}Mo_2C$ as efficient and stable catalysts for RWGS reaction", *ACS Catal.*, **7** (1), 912 (2016).

[17] Mouyane, M., Jaber, B., Bendjemil, B., Bernard, J., Houivet, D. and Noudem, J. G., "Sintering behavior of magnesium aluminate spinel $MgAl_2O_4$ synthesized by different methods", *Int. J. Appl. Ceram. Technol.*, **16** (3), 1138 (2019).

[18] Păcurariu, C., Lazău, I., Ecsedi, Z., Lazău, R., Barvinschi, P. and Mărginean., G., "New synthesis methods of $MgAl_2O_4$ spinel", *J. Euro. Ceram. Soc.*, **27** (2-3), 707 (2007).

[19] Mimani, T., "Instant synthesis of nanoscale spinel aluminates", *J. alloy. compd.*, **315** (1-2), 123 (2001).

[20] Ganesh, I., Srinivas, B., Johnson, R., Saha, B. P. and Mahajan, Y. R., "Effect of fuel type on morphology and reactivity of combustion synthesised $MgAl_2O_4$ powders", *Brit. Ceram. Trans.*, **101** (6), 247 (2002).

[21] Pati, R. K. and Pramanik, P., "Low-

temperature chemical synthesis of nanocrystalline MgAl$_2$O$_4$ spinel powder", *J. Am. Ceram. Soc.*, **83** (7), 1822 (2000).

[22] Ianoş, R. and Lazău, R., "Combustion synthesis, characterization and sintering behavior of magnesium aluminate (MgAl$_2$O$_4$) powders", *Mater. Chem. Phys.*, **115** (2-3), 645 (2009).

[23] Rodrigues, M. T., Zonetti, P. C., Alves, O. C., Sousa-Aguiar, E. F., Borges, L. E. and Appel, L. G., "RWGS reaction employing Ni/Mg (Al, Ni) O The role of the O vacancies", *Appl. Catal. A*, **543**, 98 (2017).

[24] Ojeda-Niño, O. H., Gracia, F. and Daza, C., "Role of Pr on Ni-Mg-Al mixed oxides synthesized by microwave-assisted self-combustion for dry reforming of methane", *Ind. Eng. Chem. Res.*, **58** (19),7909 (2019).

[25] Ranjbar, A., Irankhah, A. and Aghamiri, S. F., "Reverse water gas shift reaction and CO$_2$ mitigation: nanocrystalline MgO as a support for nickel based catalysts", *J. Environ. Chem. Eng.*, **6** (4), 4945 (2018).

[26] Thommes, M., Kaneko, K., Neimark, A. V., Olivier, J. P., Rodriguez-Reinoso, F., Rouquerol, J. and Sing, K. S., "Physisorption of gases, with special reference to the evaluation of surface area and pore size distribution (IUPAC Technical Report)", *Pure Appl. Chem.*, **87** (9-10), 1051 (2015).

[27] Alothman, Z.,"A review: Fundamental aspects of silicate mesoporous materials", *Mater.*, **5** (12), 2874 (2012).

[28] Li, J., Li, J., Zhu, Q., Peng, W. and Li, H., "Fabrication of hierarchical Co/MgO catalyst for enhanced CO$_2$ reforming of CH$_4$ in a fluidized-bed reactor", *AIChE J.*, **65** (1), 120 (2019).

[29] Saha, B., Khan, A., Ibrahim, H. and Idem, R., "Evaluating the performance of non-precious metal based catalysts for sulfur-tolerance during the dry reforming of biogas", *Fuel*, **120** (1), 202 (2014).

[30] Li, G., Cheng, H., Zhao, H., Lu, X., Xu, Q. and Wu, C., "Hydrogen production by CO$_2$ reforming of CH$_4$ in coke oven gas over Ni-Co/MgAl$_2$O$_4$ catalysts", *Catal. Today*, **318**, 46 (2018).

[31] Zhou, H., Cheng, H., Wu, C. and Lu, X., "Effects of nickel precursor and calcination temperature on the performance of Ni/MgAl$_2$O$_4$ catalysts for syngas production by CO$_2$ reforming of coke oven gas", *IOP Publishing, In IOP Conference Series: Materials Science and Engineering*, **381** (1), pp. 012163 (2018).

[32] Zhang, Q. and Guo, L., "Mechanism of the reverse water-gas shift reaction catalyzed by Cu 12 TM bimetallic nanocluster: A density functional theory study", *J. Clus. Sci.,* **29** (5), 867 (2018).

[33] Lortie, M., "Reverse water gas shift reaction over supported Cu-Ni nanoparticle catalysts", *Doctoral dissertation, Université d'Ottawa/ University of Ottawa*, (2014).

[34] Sun, F. M., Yan, C. F., Guo, C. Q. and Huang, S. L., "Ni/Ce-Zr-O catalyst for high CO$_2$ conversion during reverse water gas shift reaction (RWGS)", *Int. J. Hydrogen Energy*, **40** (46), 15985 (2015).